Eur. Phys. J. Plus (2025) 140:155
https://doi.org/10.1140/epjp/s13360-025-06091-9

THE EUROPEAN PHYSICAL JOURNAL PLUS

Regular Article

Dosimetric analysis of true beam linear accelerators and assessment of dosimetry of photon beams for various treatment parameters

Roya Feroze[1], Hannan Younis[1,a], Mohammad Ayaz Ahmad[2], M. Adil Khan[3], Saeed Ur Rehman[4], Shawn Jagnandan[2], Antalov Jagnandan[2], Mavia Anjum[5], Noor Ul Huda Abbasi[1], Esam M. Al-Shaebi[6], Muhammad Ajaz[7,b]

[1] Radiation Physics Lab, Department of Physics, COMSATS University Islamabad, Islamabad 45550, Pakistan
[2] Department of Mathematics, Physics and Statistics, Faculty of Natural Sciences, University of Guyana, Georgetown 101110, South America, Guyana
[3] Department of Physics, Islamia College Peshawar, Peshawar 25120, Pakistan
[4] NORI Cancer Hospital, Islamabad, Pakistan
[5] Department of Physics, University of Idaho, Moscow, Idaho, USA
[6] Department of Zoology, College of Science, King Saud University, P.O. 2455, Riyadh 11451, Saudi Arabia
[7] Department of Physics, Abdul Wali Khan University Mardan, Mardan 23200, Pakistan

Received: 21 December 2024 / Accepted: 4 February 2025

Abstract The True beam linear accelerator is a state-of-the-art device widely used in cancer treatment for its ability to deliver flattening-filter-free (FFF) and flattened photon beams. Despite its clinical significance, detailed information on its dosimetric characteristics remains limited. This study systematically evaluated dosimetric parameters for photon beam energies of 6 MV, 6 MV FFF, and 15 MV using high-resolution diode detectors and ion chambers. Measurements were conducted at a source-to-surface distance of 100 cm for field sizes ranging from 10×10 cm^2 to 40×40 cm^2 and depths of D_{max}, 5 cm, 10 cm, 20 cm, and 30 cm in water. Key metrics, including percentage depth doses (PDDs) and beam profiles, were analyzed to assess the effect of beam energy, field size, and depth on dosimetry. Comparisons of measured data from NORI Cancer Hospital and Shaukat Khanum Memorial Hospital demonstrated consistent and accurate performance across systems. These findings provide valuable insights into the dosimetric behavior of TrueBeam accelerators, contributing to the optimization of treatment protocols and ensuring improved patient outcomes.

1 Introduction

Indeed, cancer is a terrible illness that affects millions of people globally. One cancer treatment that is currently available is radiation therapy, which uses high radiation doses to kill cancerous cells and reduce tumor size. This medication can be taken either on its own or in conjunction with other therapies like chemotherapy or surgery [1]. The principle behind radiotherapy is to minimize damage to healthy tissue while using radiation to target and kill cancerous cells. This is accomplished by applying high-energy radiation to the tumor site using a device known as a linear accelerator (LINAC). Careful measurement and monitoring of the dosimetric characteristics of the treatment units are necessary to guarantee the safe and accurate delivery of radiation [2]. Dosimetry plays a crucial role in radiotherapy treatment as it provides the data necessary for treatment planning. Radiation physicists use dosimetry data to optimize treatment plans and calculate the dose for specific plans. Accurate dose calculations are essential for effective external beam radiation therapy [3–5]. The dosimetry assurance procedure for the linear accelerator is designed to ensure that the dose is delivered to the patient precisely that is intended. Even small variations in dose can have a significant impact on treatment outcomes. Correct dose estimation is essential to target cancer and neighboring tissues for the survival of adjacent organs, especially radiosensitive organs. This is crucial to avoid any serious changes in the body that could lead to the development of a second cancer [6–8]. Numerous publications in the literature discuss beam-matching result for linear accelerators [3, 9], demonstrating good dosimetric matching between similar machines [10–12]. However, similar studies specifically involving true beam accelerators are not readily available or reported in the literature.

This work presents a comparison of the percent depth dose (PDD) curves and beam profiles for photon energies (6MV, 6MV FFF, and 15MV) at five depths (Dmax, 5 cm, 10 cm, 20 cm, and 30 cm) in water at a 100 cm SSD (Source to Surface distance). The analysis was done across field sizes from 10×10 to 40×40 cm^2. The MLC (Multileaf Collimators) transmission factor is a critical parameter used to calculate the dose distribution in radiation therapy. In this study, the MLC transmission for a TrueBeam machine is $1.50\% \pm 0.05\%$ for 6 MV photon energy, $1.72\% \pm 0.06\%$ for 10 MV photon energy and $1.94\% \pm 0.07\%$ for 15 MV photon energy.

[a] e-mail: hannan.younis@comsats.edu.pk (corresponding author)
[b] e-mail: ajaz@awkum.edu.pk (corresponding author)

Published online: 24 February 2025

Fig. 1 Complete setup of TB-LINAC for dosimetry

The comprehensive dosimetric data collected from the two TB-LINAC units are indeed valuable and provide a reliable analysis of the characteristics of the new treatment system. As far as we are aware, this is the first time that the data from NORI Cancer Hospital and Shokat Khanum Memorial Hospital TB-LINACs of the same category have been compared.

2 Materials and methods

Measurements of the PDD's and Profiles have been done in two hospitals and compared by finding their standard deviation and percentage difference.

2.1 TB-linear accelerator

True beam linear accelerator is installed at NORI Cancer Hospital and Shokat Khanum Memorial Hospital (SKMH) for the treatment of cancer. The true beam linear accelerator is a medical device used in external beam radiation treatments for cancer patients. True beam linear accelerator (Fig. 1) which delivers high-energy photon beams to the targeted area with great precision, while minimizing exposure to surrounding healthy tissue. True beam is a radiotherapy machine with cutting-edge technology. It is used to deliver precise radiation therapy treatment with some millimeter's accuracy in a very short treatment time and treat tumors as large as a human body and it can be used to kill tumors as small as a few millimeters. The true beam linear accelerator featured respiratory gating with optical guidance, kV/MV imaging with CBCT (cone-beam computed tomography) capability, 120 MLC, and real-time imaging during treatment delivery is used in this work [13].

2.2 Scanning water phantom

Scanning water phantoms is commonly used to collect scanned beam data in radiotherapy. It can be seen from Fig. 2 that these phantoms consist of a plastic tank filled with water, which is deep enough to allow for central axis PDD and profile measurements to be taken up to a depth of 40 cm and 40 cm in width. The photon beam scanning system needs to be able to scan in the x and y directions to avoid any problems that may arise due to tank rotation. This ensures accurate and precise scanning results [14]. Symmetry calibration for photons (and electrons) was performed in a water phantom at energies of 6MV, 6MV FFF, and 15MV, at five different depths (Dmax, 5 cm, 10 cm, 20 cm, and 30 cm) in water, with a source-to-surface distance (SSD) of 100 cm. The analysis was conducted across field sizes ranging from 10×10 cm^2 to 40×40 cm^2. Symmetry calibration is performed to adjust beam steering and achieve optimal symmetry values. The tissue phantom ratio (TPR) was also used for energy matching and symmetry calibration.

2.3 Ion chambers

Ionization chambers have been used in radiation measurement since the discovery of radiation, and they remain a popular choice today due to their consistent response to energy, dose rate, dose, and reproducibility. Figure 3 shows an ion chamber that we have used for data collection. They work by measuring the electrical charge produced when ionizing radiation passes through a gas-filled chamber. This charge is then measured and used to calculate the dose of radiation delivered. Ionization chambers are widely used in clinical settings to ensure accurate and consistent radiation dosimetry. Ion chambers are indeed a cost-effective and easily accessible option for radiation detection [15]. They come in different shapes such as spherical, cylindrical, and parallel plate, and sizes like standard, mini, and micro, making them versatile for various applications. Some types of ionization chambers are Semi-flex for

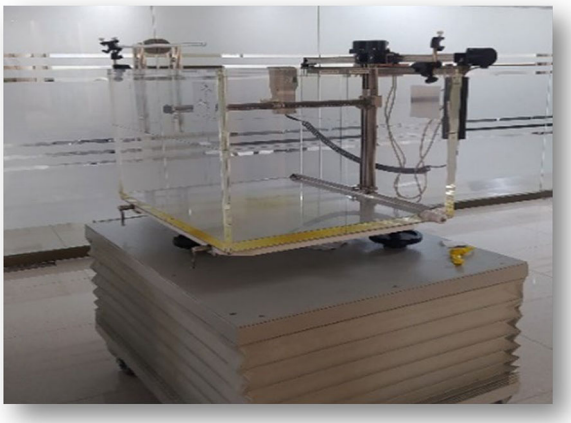

Fig. 2 Water phantom for LINAC dosimetry

Fig. 3 Ionization chamber used in dose measurement

field sizes above 4×4 cm^2, Diode/Pinpoint for small field sizes 2×2 to 4×4 cm^2 and Farmer chamber. In the dosimetry of true beam LINAC, two chambers that are used for dose monitoring are the main chamber and the reference chamber. Both are ionization chambers for effective radiation therapy treatment delivery. Both the main chamber and reference chamber play an essential role.

2.4 Diodes detectors

Diode detectors are the preferred choice for beam data commissioning, as they provide several remarkable advantages. They offer high sensitivity, excellent spatial resolution, and quick response time in microseconds, without any external bias. These characteristics make them a good device in the field of radiation detection and measurement [16]. By using diode detectors, data collection becomes more accurate and reliable, which is crucial for successful external beam radiation therapy. The response of diode detectors is affected by various factors such as SSD or wedge, temperature, dose rate, and energy. Therefore, it is essential to consider these factors when selecting and using diode detectors for radiation detection and measurement.

2.5 Beam generation

Electrons are accelerated to high energies using a sequence of accelerating structures in a linear accelerator (LINAC) and then they are directed toward a target composed of a high atomic number material, like gold or tungsten. Bremsstrahlung radiation is the term for the high-energy photons that are produced when electrons collide with a target. Then in order to target cancer cells with the least amount of exposure to healthy tissue, this photon beam is shaped and directed toward the patient. The photon beam's energy is meticulously regulated to guarantee that it is adequate to eradicate cancer cells while causing the least amount of harm to the surrounding healthy tissue. The energy of the photons can be adjusted by changing the energy of the accelerated electrons and the thickness of the target material [17].

2.6 Beam collimation

Beam collimation is the process of shaping and restricting the size of the radiation beam according to the size and shape of the cancer. This is done to minimize the effect of radiation to healthy tissues that are exposed to the radiation and to maximize the dose to the cancer. Collimation is achieved by using a series of collimators, which are devices that can be adjusted to shape and restrict the size of the beam. The primary collimator, located close to the target, shapes the beam to match the size and shape of the cancer. The secondary collimators, located further away from the target, further restrict the size of the beam and shape it to match the desired treatment field. Wedges, flattening filters, and MLCS are also used to shape the beam [18].

2.7 Percentage depth dose (PDD)

The percentage depth dose (PDD) is a crucial factor in radiation therapy treatment planning. At each depth, the PDD indicates the percentage of the maximum dose delivered to that depth, and it varies for different organs. A PDD curve is generated by plotting the percentage dosage against depth, providing valuable information on the dosage distribution within the substance as a function of depth. This curve helps determine the amount of dosage delivered at different levels and how deeply the radiation penetrates. PDD curves ensure that the recommended dose is accurately delivered to the target while minimizing damage to nearby healthy tissue [8]. To calculate the maximum delivered dose of a radiation beam at a specific depth within a material, such as the human body, the percentage depth dose formula is typically used,

$$\mathrm{PDD} = \frac{D_{\mathrm{d}}}{D_{\max}} \times 100\%$$

where dose at the depth D_{d} is the exact dose administered at the depth of interest and maximum dosage $D_{\max}$ is the highest dosage of radiation that can be delivered by the radiation beam, usually at the material's surface.

2.8 Beam profiles

To guarantee that the radiation beam is evenly distributed and conforms to the required shape, it is crucial to assess the spatial distribution of radiation dose across the treatment area. Specialized detectors or film positions are used in the therapy beam path to distribute the beam uniformly. These measurements help to guarantee that the treatment is administered precisely and safely by offering important information about the distribution of radiation doses [8].

2.9 Off-axis factor

Off-axis factor is an important parameter in radiation therapy as it helps to determine the dose distribution of the radiation beam away from the central axis. The OAF is affected by various factors such as the energy of the beam, the distance from the source, and the size of the field.

Mathematically:

$$\mathrm{OAF} = \frac{D_{\text{off axis}}}{D_{\text{Central axis}}}$$

$D_{\text{off axis}}$ is the dose at the off-axis and the $D_{\text{central axis}}$ is the dose at the central axis.

2.10 Data comparison of two hospitals

The PDD's and profiles of both NORI Cancer Hospital and Shaukat Khanam Memorial Hospital (SKMH) using true beam linear accelerator data have been calculated. Further, the data are compared from both hospitals to evaluate the performance of the linear accelerators. The percentage difference between the two hospitals' data are also calculated, which is a useful metric to determine the level of agreement between the two datasets. Additionally, this study also calculated the standard deviation (S.D) of SKMH data from NORI data, which can provide insight into the variability of the data.

2.10.1 Standard deviation (S.D)

One important statistical tool for assessing how much variation or dispersion there is in a set of values is the standard deviation [19]. A high standard deviation signifies the values are distributed over a wider range from the mean, whereas a low standard deviation implies that the values are concentrated around the mean or average value. The formula for standard deviation is:

$$\mathrm{S.D} = \sum \sqrt{\frac{(x_i - \mu)^2}{N}}$$

where N is the total number of values in the data set, μ is the mean of the data set, and Xi is each value in the data set.

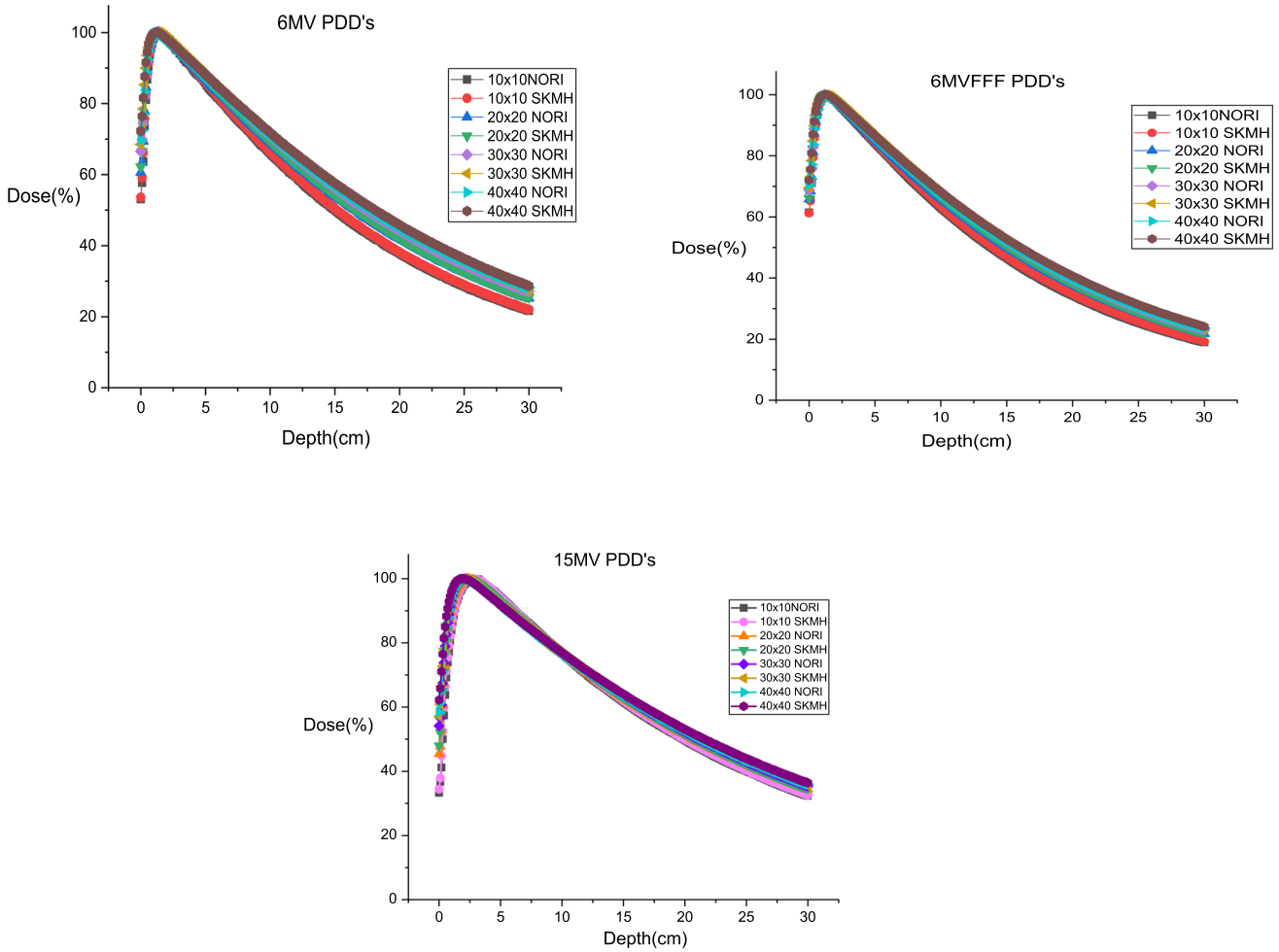

Fig. 4 PDDs comparison of SKMH and NORI Hospital for 6MV, 6MV FFF, and 15MV

2.10.2 Percentage difference

It is the relative difference between two values that can be expressed as a percentage of one of those values.

Mathematically:

$$\text{Percentage difference} = \frac{(\text{Value}_1 - \text{Value}_2)}{\text{Value}_1} \times 100$$

where value_1 is the reference value and value_2 is the value, we want to compare with the reference value.

3 Results and discussion

Figure 4 shows that the dose decreases as the depth increases, and as a result, the maximum dose will be delivered at the surface. The area where the dose value is maximum is known as the buildup region. Before and after the buildup region, the dose will be less. It is also clear from Fig. 4 that with the increase in field size, the dose increases.

The percentage difference of Shaukat khanum from NORI hospital for 6MV for field size 10×10 (cm^2) values before $D_{\max}$ (1.5) and after $D_{\max}$ (1.5) is 1.07 ± 0.93 and 0.80 ± 0.32, respectively. The values for other field sizes and energies are given in Table 1.

Typically, the central axis of the beam profile represents the maximum dose, also known as the peak dose. This peak dose is dependent on both the beam energy and the field size, higher peak doses being produced by beams with higher energy and smaller field sizes.

6MV FFF (Flattening filter free beam) graph shows that removing the filter will result in the delivery of more doses at the center of the axis and less at the periphery. However, using a filter can help obtain a uniform dose profile.

Table 1 PDDs of 6MV, 6MV FFF, and 15MV percentage difference and standard deviation of SKMH from NORI Hospital

Percentage depth dose (PDD)	10×10 (cm^2)	20×20 (cm^2)	30×30 (cm^2)	40×40 (cm^2)
6MV				
Before D_{max} (1.5)	1.07 ± 0.93	1.88 ± 0.24	1.59 ± 0.26	1.94 ± 0.39
After D_{max}(1.5)	0.80 ± 0.32	0.68 ± 0.26	0.69 ± 0.20	0.78 ± 0.23
6MV FFF				
Before Dmax(1.2)	0.30 ± 0.13	1.02 ± 0.34	1.02 ± 0.80	1.83 ± 0.33
After Dmax(1.2)	1.12 ± 0.46	1.04 ± 0.47	1.10 ± 0.55	1.08 ± 0.62
15MV				
Before Dmax(2.8)	1.64 ± 0.02	2.47 ± 1.57	2.15 ± 1.46	2.21 ± 1.48
After Dmax(2.8)	0.36 ± 0.11	0.43 ± 0.23	0.32 ± 0.20	0.38 ± 0.24

Table 2 6MV, 6MV FFF, and 15MV profiles percentage difference and standard deviation of SKMH from NORI Hospital at D_{max}

Parameters	10×10 6MV	10×10 6MV FFF	10×10 15MV
Out of field	6.24 ± 2.50	6.09 ± 2.46	3.36 ± 1.60
Penumbra	6.35 ± 2.51	6.24 ± 2.49	5.24 ± 2.08
In-field	0.23 ± 0.27	0.22 ± 0.11	0.17 ± 0.10

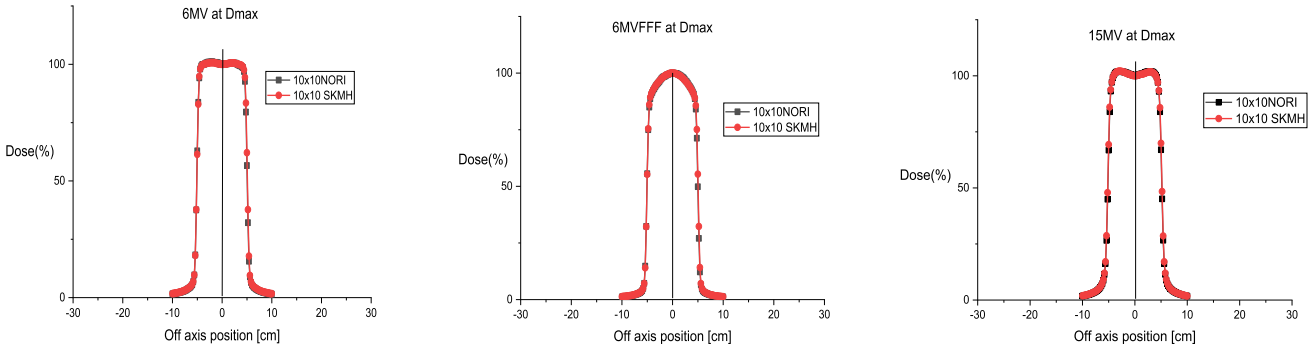

Fig. 5 Comparison of SKMH and NORI Hospital for 6MV, 6MV FFF, and 15MV at D_{max} depth

Out of field, Penumbra, and in-field percentage difference and standard deviation values for 6MV beam profile for 10×10 cm^2 at Dmax are 6.24 ± 2.50, 6.35 ± 2.51 and 0.23 ± 0.27, respectively, and the other values for different energies are given in Table 2. Penumbra refers to the area where the dose falls off quickly and it is also called the transition region as shown in Fig. 5. In-field refers to the region where data points are within the treatment field, and out of field refers to the area where data points lie outside of the treatment field (Fig. 5).

It can be seen in Fig. 6 that, as we move off-axis in an open field, there can be little horns on the edge that go up a bit. However, as we move deeper into the phantom, these profiles become more rounded off and smoother, resulting in a more uniform beam. It shows that the increase in field size contributes to the improved uniformity of the beam. Out of field, Penumbra and in-field percentage difference and standard deviation values for 6MV for 10×10 cm^2 at 5 cm are 3.02 ± 1.47, 5.70 ± 2.38, and 0.32 ± 0.02, respectively, and the values for other energies and field sizes at 5 cm are given in Table 3.

Fields are almost overlapping, which means that both hospitals' beam profile data is almost the same, as can be seen in Fig. 7.

Out of field, Penumbra, and in-field percentage difference and standard deviation values for 6MV FFF for 10×10 cm^2 at 10 cm are 1.93 ± 0.27, 3.48 ± 1.86 and 0.22 ± 0.13, respectively, and the values for other energies and field sizes at 10 cm are given in Table 4. It is clear that the standard deviation values are not too high which means that both hospital data are almost similar.

In small field sizes, the penumbra width can be relatively small. Due to the relatively steep penumbra, it can be difficult to achieve a steep dose gradient at the field borders in small fields, which makes it more difficult to precisely target cancers while protecting nearby healthy tissues. Large penumbra is present in larger field sizes. A major section of the field undergoes the transition from high to low dose. The wide penumbra of large fields can be advantageous when treating larger target volumes because it allows for a more gradual dose falloff at the field's boundaries, reducing the possibility of excess dose or insufficient dose delivery to the surrounding tissues.

Figure 8 shows out of field, Penumbra, and in-field percentage difference and standard deviation values for 6MV FFF for 10×10 cm^2 at 20 cm are 2.69 ± 0.91, 2.64 ± 1.62, and 0.20 ± 0.13, respectively, and the values for other energies and field sizes at 20 cm are given in Table 5.

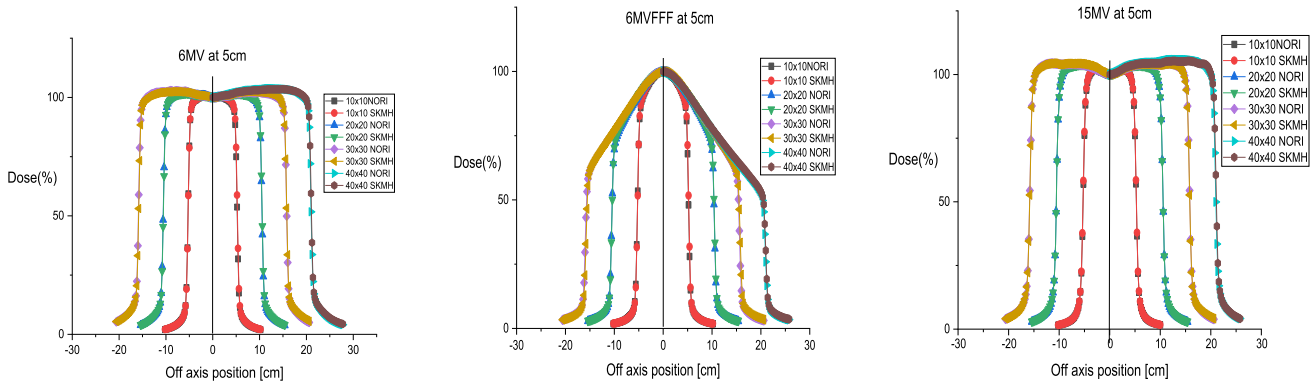

Fig. 6 Comparison of SKMH and NORI Hospital for 6MV, 6MV FFF, and 15MV at 5 cm depth

Table 3 6MV, 6MV FFF, and 15MV profiles percentage difference and standard deviation of SKMH from NORI Hospital at 5 cm

Parameters	10×10 cm^2	20×20 cm^2	30×30 cm^2	40×40 cm^2
6MV				
Out of field	3.02 ± 1.47	2.83 ± 1.29	3.66 ± 1.91	3.73 ± 1.38
Penumbra	5.70 ± 2.38	5.18 ± 1.79	7.25 ± 2.17	8.89 ± 2.98
In the field	0.32 ± 0.02	0.18 ± 0.09	0.28 ± 0.13	0.19 ± 0.09
6MV FFF				
Out of field	1.97 ± 0.17	2.40 ± 0.24	6.16 ± 2.48	2.59 ± 0.19
Penumbra	4.85 ± 2.20	1.83 ± 0.35	2.85 ± 0.68	1.15 ± 0.44
In the Field	0.26 ± 0.07	0.24 ± 0.14	0.13 ± 0.07	0.11 ± 0.06
15MV				
Out of Field	2.37 ± 1.38	1.79 ± 1.22	1.98 ± 0.18	2.48 ± 1.39
Penumbra	2.58 ± 0.48	0.67 ± 0.38	2.51 ± 0.57	5.44 ± 1.92
In the Field	0.23 ± 0.18	0.13 ± 0.08	0.20 ± 0.03	0.42 ± 0.18

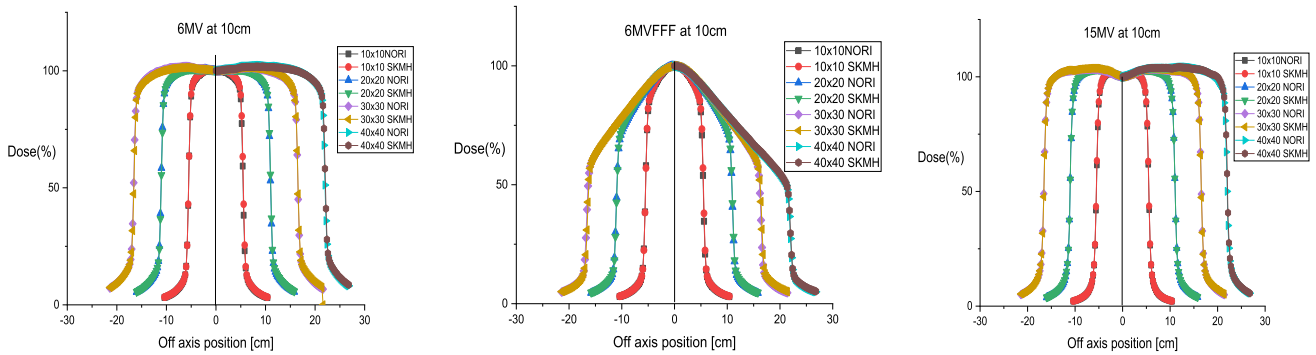

Fig. 7 Comparison of SKMH and NORI Hospital for 6MV, 6MV FFF, and 15MV at 10 cm depth

As we can see from Fig. 9, with the increase in depth beam uniformity increases and higher energy beams radiation often penetrates tissues more deeply.

Out of field, Penumbra, and in-field percentage difference and standard deviation values for 15MV for 10×10 cm^2 at 30 cm are 4.02 ± 1.41, 2.03 ± 0.71, and 0.17 ± 0.04, respectively, and the values for other energies and field sizes at 30 cm are given in Table 6. The standard deviation is less than 10% for all the values which increases the authenticity of data. Small standard deviation values mean fewer data are deviating from the mean value and large standard deviation means more data are deviating from the mean value.

Table 4 6MV, 6MV FFF, and 15MV profiles percentage difference and standard deviation of SKMH from NORI Hospital at 10 cm

Parameters	10×10 cm^2	20×20 cm^2	30×30 cm^2	40×40 cm^2
6MV				
Out of Field	3.09 ± 1.46	2.58 ± 1.25	3.36 ± 1.74	3.59 ± 0.79
Penumbra	4.51 ± 2.12	3.90 ± 1.60	4.91 ± 2.12	9.38 ± 3.49
In the field	0.41 ± 0.25	0.15 ± 0.09	0.26 ± 0.14	0.33 ± 0.13
6MV FFF				
Out of Field	1.93 ± 0.27	2.42 ± 0.83	5.40 ± 2.32	2.91 ± 0.71
Penumbra	3.48 ± 1.86	1.30 ± 0.36	2.23 ± 0.49	0.70 ± 0.82
In the Field	0.22 ± 0.13	0.26 ± 0.12	0.19 ± 0.08	0.21 ± 0.09
15MV				
Out of Field	2.18 ± 1.18	1.21 ± 0.75	2.18 ± 1.12	1.46 ± 0.70
Penumbra	1.95 ± 0.33	0.96 ± 0.32	1.76 ± 0.71	10.57 ± 3.25
In the Field	0.18 ± 0.06	0.10 ± 0.07	0.26 ± 0.13	0.24 ± 0.03

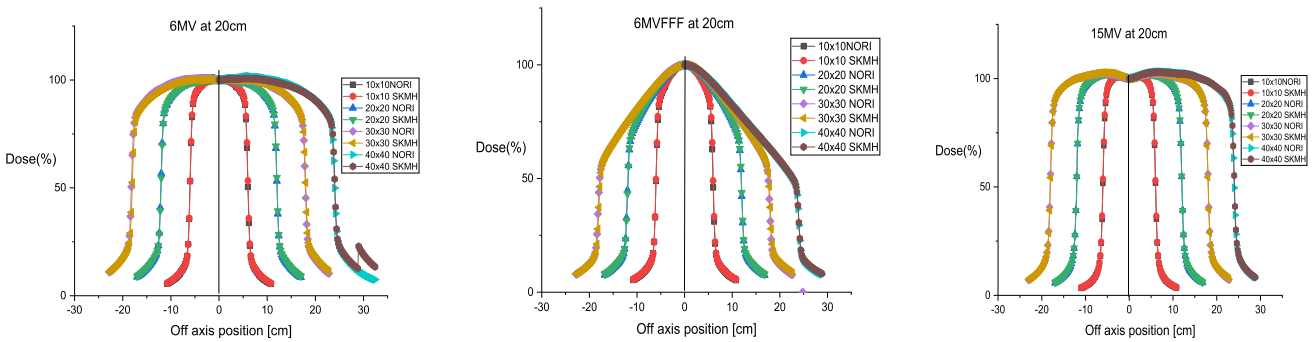

Fig. 8 Comparison of SKMH and NORI Hospital for 6MV, 6MV FFF, and 15MV at 20 cm depth

Table 5 6MV, 6MV FFF, and 15MV profiles percentage difference and standard deviation of SKMH from NORI Hospital at 20 cm

Parameters	10×10	20×20	30×30	40×40
6MV				
Out of Field	0.40 ± 0.19	3.44 ± 1.03	4.93 ± 2.22	3.36 ± 1.83
Penumbra	1.06 ± 0.75	1.94 ± 1.20	9.43 ± 3.07	3.85 ± 1.96
In the field	0.17 ± 0.10	0.20 ± 0.13	0.41 ± 0.27	0.67 ± 0.23
6MV FFF				
Out of Field	2.69 ± 0.91	3.15 ± 0.81	4.48 ± 2.11	3.17 ± 0.70
Penumbra	2.64 ± 1.62	0.89 ± 0.39	2.04 ± 0.42	0.57 ± 0.28
In the Field	0.20 ± 0.13	0.25 ± 0.08	0.14 ± 0.07	0.49 ± 0.19
15MV				
Out of Field	2.59 ± 1.20	2.25 ± 1.05	2.74 ± 0.97	0.60 ± 0.50
Penumbra	2.22 ± 0.76	0.59 ± 0.27	1.49 ± 0.59	6.71 ± 2.59
In the Field	0.17 ± 0.11	0.17 ± 0.08	0.25 ± 0.13	0.24 ± 0.14

4 Conclusion

In this study, the PDD's and profiles of true beam LINACs from two hospitals of the same category were measured and compared to ensure accuracy. This comparison is crucial for identifying any discrepancies and ensuring uniformity in the measurements. All the measured data fall within the specified limits provided by Varian, with a standard deviation below 10% for 6MV, 6MV FFF, and 15MV. These results demonstrate that the LINACs in these two hospitals are suitable for clinical practice. Proper selection of these parameters is essential to ensure the safe and effective delivery of rasdiation therapy while minimizing the risk to healthy tissues.

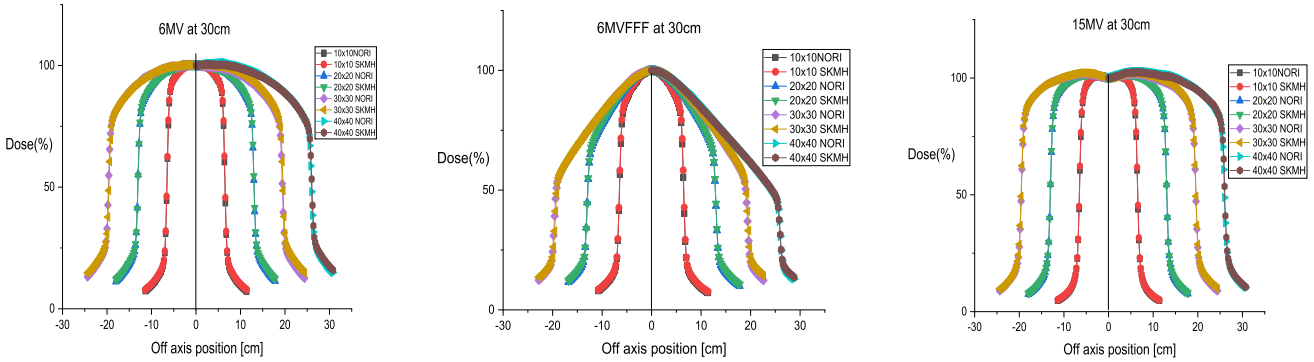

Fig. 9 Comparison of SKMH and NORI Hospital for 6MV, 6MV FFF, and 15MV at 30 cm depth

Table 6 6MV, 6MV FFF, and 15MV profiles percentage difference and standard deviation of SKMH from NORI Hospital at 30 cm

Parameters	10×10 cm^2	20×20 cm^2	30×30 cm^2	40×40 cm^2
6MV				
Out of Field	5.31 ± 1.14	5.40 ± 1.01	11.25 ± 2.57	5.73 ± 0.55
Penumbra	2.69 ± 0.86	2.09 ± 0.35	7.67 ± 2.76	3.73 ± 1.21
In the field	0.24 ± 0.12	0.40 ± 0.37	0.50 ± 0.33	0.59 ± 0.18
6MV FFF				
Out of Field	3.69 ± 0.79	4.42 ± 0.57	9.38 ± 2.64	4.96 ± 0.59
Penumbra	2.64 ± 1.09	0.70 ± 0.45	1.88 ± 0.37	0.48 ± 0.28
In the Field	0.21 ± 0.04	0.17 ± 0.11	0.15 ± 0.09	0.62 ± 0.24
15MV				
Out of Field	4.02 ± 1.41	2.87 ± 0.84	6.49 ± 1.19	0.83 ± 0.39
Penumbra	2.03 ± 0.71	0.67 ± 0.28	3.31 ± 1.34	4.64 ± 2.15
In the Field	0.17 ± 0.04	0.08 ± 0.01	0.35 ± 0.10	0.51 ± 0.18

Acknowledgements This work was supported by the Researchers Supporting Project number (RSPD2025R1079) at King Saud University (Riyadh, Saudi Arabia). The authors also express their gratitude to Nori Cancer Hospital and SKMH for their support throughout the beam data measurement period.

Data Availability Statement The data supporting this study are available from the corresponding author upon reasonable request. The manuscript has associated data in a data repository

Declarations

Conflict of interest No conflict of interest.

References

1. S.M. Bentzen, Preventing or reducing late side effects of radiation therapy: Radiobiology meets molecular pathology. Nat. Rev. Cancer **6**(9), 702–713 (2006)
2. B. Dutta, S. Goswami, S. Moran, P. Talukdar, Commissioning and performance evaluation of Varian Truebeam linear accelerator. J. Radiat. Med. Tropics **4**(1), 25 (2023). https://doi.org/10.4103/jrmt.jrmt_11_22
3. M. Ghazal, L. Södergren, M. Westermark, J. Söderström, T. Pommer, Dosimetric and mechanical equivalency of Varian TrueBeam linear accelerators. J. Appl. Clin. Med. Phys.Clin. Med. Phys. **21**(12), 43–53 (2020). https://doi.org/10.1002/acm2.13058
4. J. Chen, Q. Chen, P. Xiao, W. Jin, L. Yu, A novel framework for uncovering the coordinative spectrum-effect correlation of the effective components of Yangyin Tongnao Granules on cerebral ischemia-reperfusion injury in rats. J. Ethnopharmacol.Ethnopharmacol. **337**, 118844 (2025). https://doi.org/10.1016/j.jep.2024.118844
5. Y. Guo, Z. Han, J. Zhang, L. Yue, C. Li, G. Liu, Development of a high-speed and ultrasensitive UV/Vis-CM for detecting total triterpenes in traditional Chinese medicine and its application. Heliyon **10**(11), e32239 (2024). https://doi.org/10.1016/j.heliyon.2024.e32239
6. D. De Ruysscher, G. Niedermann, N.G. Burnet, S. Siva, A.W.M. Lee, F. Hegi-Johnson, Radiotherapy toxicity. Nat. Rev. Disease Prim. (2019). https://doi.org/10.1038/s41572-019-0064-5
7. Z. Chang, Q. Wu, J. Adamson, L. Ren, J. Bowsher, H. Yan, A. Thomas, F.-F. Yin, Commissioning and dosimetric characteristics of TrueBeam system: Composite data of three TrueBeam machines. Med. Phys. **39**(11), 6981–7018 (2012). https://doi.org/10.1118/1.4762682
8. L. C. Matsushima, G. R. Veneziani, P. A. Piedade, W. G. Maia, P. T. V. N. Filho, Comparison of parameters related on beam profile, PDDs and output factor from commissioning data of linear accelerators TrueBeam®. 567, (2019).

9. Q. Zhang, J. Liu, N. Ao, Y. Hui, Y. Peng, O. Liya, S. Zhang, Secondary cancer risk after radiation therapy for breast cancer with different radiotherapy techniques. Sci. Rep. (2020). https://doi.org/10.1038/s41598-020-58134-z
10. Z. Jiang, Y. Li, Z. Wei, B. Yuan, Y. Wang, O.U. Akakuru, A. Wu, Pressure-induced amorphous zeolitic imidazole frameworks with reduced toxicity and increased tumor accumulation improves therapeutic efficacy In vivo. Bioactive Mater. **6**(3), 740–748 (2021)
11. S. Liu, F. Meng, S. Guo, M. Yuan, H. Wang, X. Chang, Inhibition of α-amylase digestion by a Lonicera caerulea berry polyphenol starch complex revealed via multi-spectroscopic and molecular dynamics analyses. Int. J. Biol. Macromol.Macromol. **260**, 129573 (2024). https://doi.org/10.1016/j.ijbiomac.2024.129573
12. Z. Zhang, L. Wang, Z. Guo, Y. Sun, J. Yan, A pH-sensitive imidazole grafted polymeric micelles nanoplatform based on ROS amplification for ferroptosis-enhanced chemodynamic therapy. Colloids Surf. B **237**, 113871 (2024). https://doi.org/10.1016/j.colsurfb.2024.113871
13. K.N. Kielar, E. Mok, A. Hsu, L. Wang, G. Luxton, Verification of dosimetric accuracy on the TrueBeam STx: Rounded leaf effect of the high definition MLC. Med. Phys. **39**(10), 6360–6371 (2012). https://doi.org/10.1118/1.4752444
14. C. Glide-Hurst, M. Bellon, R. Foster, C. Altunbas, M. Speiser, M. Altman, D. Westerly, N. Wen, B. Zhao, M. Miften, I.J. Chetty, T. Solberg, Commissioning of the Varian TrueBeam linear accelerator: A multi-institutional study. Med. Phys. **40**(3), 031719 (2013). https://doi.org/10.1118/1.4790563
15. Design of parallel plate ion chambers for buildup measurements in megavoltage photon beams—Rawlinson—1992—Medical Physics—Wiley Online Library. (n.d.). Retrieved December 16, 2023, from https://aapm.onlinelibrary.wiley.com/doi/abs/https://doi.org/10.1118/1.596896?casa_token=V7IPlg4jdm0AAAAA:ZRuo1DZwcHNJFTVCIQDKDrzYHICJdP38NYhESdrZeS3-FEX7BI3wA91FaGv379-Mc76U8KdLlLcNGdj1
16. Dosimetric Characteristics of a PIN Diode for Radiotherapy Application—Rajesh Kumar, S. D. Sharma, A. Philomina, Anita Topkar, 2014. (n.d.). Retrieved December 16, 2023, from https://journals.sagepub.com/doi/abs/https://doi.org/10.7785/tcrt.2012.500388
17. D. Parsons, M. Joo, Z. Iqbal, A. Godley, N. Kim, A. Spangler, K. Albuquerque, A. Sawant, B. Zhao, G. Xuejun, A. Rahimi, Stability and reproducibility comparisons between deep inspiration breath-hold techniques for left-sided breast cancer patients: A prospective study. J. Appl. Clin. Med. Phys.Clin. Med. Phys. **24**, 5 (2023)
18. A Simple lnterferometric Method of Beam Collimation. (n.d.). Retrieved December 16, 2023, from https://opg.optica.org/ao/abstract.cfm?uri=ao-10-8-1980_1
19. Estimating the sample mean and standard deviation from the sample size, median, range and/or interquartile range | BMC Medical Research Methodology. (n.d.). Retrieved December 15, 2023, from https://link.springer.com/article/https://doi.org/10.1186/1471-2288-14-135